Observation and Analysis of Model Lipid Raft Deformation Dynamics Induced by Lipoprotein–Gold Nanorod-based Devices to Manipulate Phase Transition of Lipid Bilayer

Tomohiro Nobeyama[a*] and Tatsuya Murakami[b]

[a] Faculty of Pure and Applied Sciences, University of Tsukuba, 1-1-1 Tennodai, Tsukuba, Ibaraki 305-8573, Japan

[b] Graduate School of Engineering, Toyama Prefectural University, 5180 Kurokawa, Imizu, Toyama 939-0398 Japan

*nobeyama.tomohiro.fu@u.tsukuba.ac.jp

Abstract

Lipid rafts, which are complexes that form on cholesterol-rich areas of cell membranes, play key roles as gates for the distribution of information between the inner and outer spaces of living cells. The physical and biological properties of lipid rafts have been investigated, but the engineering of lipid rafts remains a difficult subject. We developed a lipoprotein–gold nanorod nanodevice to control the formation/deformation of model lipid rafts. The nanodevice attached to the liquid order (Lo) phase region, selectively removed cholesterol from the Lo domain, and induced the Lo-to-solid order (So) phase transition. In this study, we analyzed the phase transition induced by the nanodevice. We found that the domain boundary gradually collapsed and that a local two-phase mixture was induced. Local instability resulted in domain incursion into other domains, and protrusions were torn to form small domains with the characteristics of two phases. The two different domains grouped together to form a non-circular So domain on giant unilamellar vesicles. Close observation of the non-equilibrium process of phase transition may lead to the design of strategies for external lipid raft manipulation methodology using biological macromolecules and/or nanoparticles.

Introduction

All cells are surrounded by a lipid bilayer membrane that serves as an interface between the inner and outer cellular spaces.[1,2] The physical properties of the lipid bilayer membrane play key roles in the function of the interface. Since the 1980s, the compartments of the cell membrane and model membranes have been studied.[3–6] In 1997, a cholesterol- and sphingolipid-rich area called

lipid raft was reported, and there has been a lot of evidence to show that the lipid raft is a small domain-like structure that forms as a result of phase separation in the lipid bilayer membrane.[7]

The lipid bilayer membrane has three typical phases, namely the fluidic area that contains unsaturated lipid molecules and is known as the Liquid order (Ld) phase region, the non-fluidic area that contains saturated lipid molecules and is known as the Solid order (So) phase region, and the cholesterol-rich liquid area known as the Liquid order (Lo) phase region. The Lo phase region has been used as a model of lipid rafts. Further, giant unilamellar vesicles (GUVs), which contain domains of the Lo and Ld phase regions, are often used as models for the analysis of characteristics of lipid rafts.[8]

There is a lot of evidence regarding the significance and universality of lipid rafts. For example, it was reported that lipid rafts are related to immune signaling and immune cell activation,[9–11] secretion of proteins such as insulin,[12] brain aging,[13] cancer cell adhesion,[14] and regulation of some transient receptor potential channels related to heat, cooling, and pain.[15,16] Model membrane experiments revealed that some viruses, such as human immunodeficiency virus and severe acute respiratory syndrome coronavirus 2, may infect human cells by adhering to the boundary of lipid rafts.[17,18] Lipid rafts exist on plasma membranes of mammalian cells as well as on plant cell membranes.[19] Recent studies reported that lipid rafts also exist on cell organelles such as mitochondria, Golgi apparatus, and chloroplasts.[20–22]

Manipulation of the formation/deformation of model lipid rafts may be an important methodology in cell engineering; however, most previous studies focused on the equilibrium state of lipid rafts. Thus, it is difficult to design control methods. The dynamic process associated with lipid rafts in vivo probably occurs in a non-equilibrium state; therefore, it is necessary to study the non-equilibrium process.[23–25]

There are only a few studies on non-equilibrium processes of domain formation/deformation such as membrane fusion and lipid diffusion.[26–29] Furthermore, not many studies have investigated the interaction between the interface and GUVs for domain formation/deformation.[30–32]

Recently, we developed the first biocompatible nanodevice to regulate the formation/deformation of model lipid rafts.[30] The nanodevice is composed of a gold nanorod (AuNR) and a cationic high-density lipoprotein (HDL) (Figure 1A).[33,34] The surface of the AuNR was coated with an HDL-originated lipid–protein complex layer. HDLs serve as carriers of cholesterol in the human body

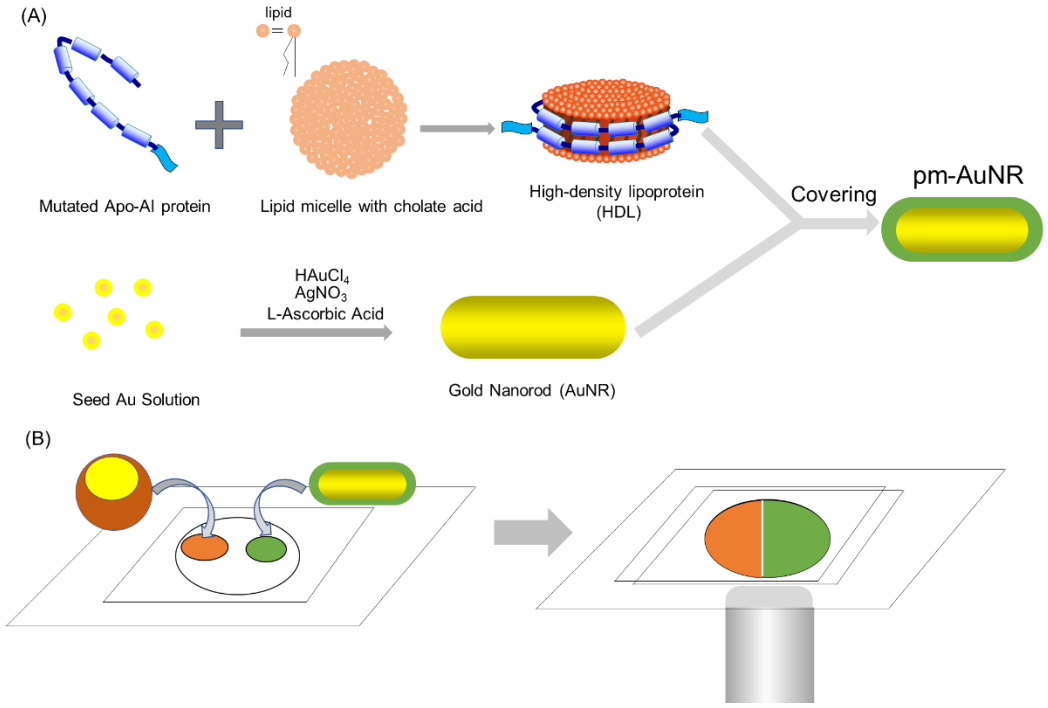

Figure 1. (A) Schematic image of pm-AuNR preparation: biologically prepared reconstituted Apo-AI protein and a lipid micelle are co-incubated to form a lipoprotein. The reconstituted Apo-AI protein has a TAT peptide sequence at its C-terminal that increases membrane affinity. The high-density lipoprotein is used to cover the AuNR surface to form a pm-AuNR. The surface has high affinity with a lipid bilayer surface and causes Lo/Ld phase transition on lipid bilayers. (B) Schematic image of the microscopic system for detailed observation of phase transition: dropped GUVs and pm-AuNR dispersants on a thin silicon chamber were squashed lightly with a cover glass to make a boundary of the two solutions. The delayed phase transition on the boundary was observed using a fluorescent microscope.

and as modulators of lipid rafts, and cholesterol affinity reduces inflammation by cholesterol efflux from B cells.[35] AuNR has high stability, low toxicity, good size-modification capability, and a photothermal effect for local heating.[36] The nanodevice we developed was a plasma membrane-targeted AuNR (pm-AuNR). We showed that the nanodevice can control Lo-to-So phase transition by cholesterol absorption and material adhesion and that it photo-regulates So-to-Lo phase transition induced by cholesterol supplements from previously prepared cholesterol-saturated pm-AuNRs.[30]

In this study, we evaluated the phase transition process triggered by pm-AuNRs and analyzed the morphological changes of Lo domains through phase transition. We monitored the phase separation process and found that the domain boundary was unsettled and mixed in some local areas. Thereafter, the Lo and Ld domains mixed with each other near the unstable areas, and microdomains formed in the Lo or So phase region. The domains gradually joined together and formed uncirculated So domains on the GUVs.

Experimental

General Information

General reagents were purchased from Nacalai Tesque Inc. (Kyoto, Japan). Gold (III) chloride and sodium borohydride (NaBH4) were purchased from Sigma-Aldrich Inc. (Saint Louis, MO, USA). Silver nitrate, L-(+)-ascorbic acid, and sodium oleate were purchased from Wako Pure Chemicals Inc. (Osaka, Japan). We obtained 1-palmitoyl-2-oleoyl-sn-glycero-3-phosphocholine (POPC) from NOF Co. Ltd. (Tokyo, Japan). Further, we purchased 1,2-dioleoyl-3-trimethylammonium-propane (DOTAP), 1,2-dioleoyl-sn-glycero-3-phosphoethanolamine-N-(7-nitro-2-1,3-benzoxadiazol-4-yl) (NBD-PE), and 1,2-dipalmitoyl-sn-glycero-3-phosphoethanolamine-N-(lissamine rhodamine B sulfonyl) (Rhodamine-PE) from Avanti Polar Lipids Inc. (Alabaster, AL, USA). Cholesterol and indium tin oxide (ITO) glasses were purchased from Sigma-Aldrich Inc. (Saint Louis, MO, USA). Visible/near-infrared spectra were measured using the V-630 spectrometer (JASCO Corporation, Tokyo, Japan). AuNRs were synthesized or obtained from Dai Nippon Toryo Co. Ltd. (Osaka, Japan). Images of GUVs were obtained using a Zeiss LSM 800 confocal fluorescent microscope. The concentration of the cationic HDL mutant (catHDL) on protein basis was measured using a DC Protein Assay kit (Bio-Rad Laboratories, CA, USA). The hydrodynamic diameter of catHDL was measured using a Nanotrack UPA-UT151 apparatus (Microtrack Bell Co. Ltd., Osaka, Japan).

catHDL preparation

The preparation of catHDL was described in a previous report[30,33]. In brief, POPC and DOTAP solutions in ethanol were mixed in a round-bottom flask in a molar ratio of 7:3. A 6 mol% solution of NBD-PE in ethanol was added if necessary. The reaction mixture was concentrated and dried under reduced pressure for at least two hours to remove all solvents. The lipid film was dispersed in a 3-mg/mL sodium cholate solution in phosphate-buffered saline (PBS, pH 7.4). Following incubation at 37℃ for at least two hours, the recombinant apolipoprotein AI (Apo-AI) mutant with a deleted N-terminal 43-amino acid fragment and a cell-penetrating TAT peptide fused at the C-terminal were mixed at a protein-to-lipid molar ratio of 100 in PBS containing 4 M urea. The reaction mixture was incubated at room temperature overnight. The mixture containing catHDL was dialyzed against 3 L of PBS for at least four hours, changing the dialysate three times

to remove urea, sodium cholate, and unreacted proteins. The sample was then centrifuged to remove debris.

Synthesis of AuNRs coated with hexadecyltrimethylammonium bromide (CTAB)

AuNRs were synthesized by the seedless method.[30,53] In this method, 1200 µL of a 4-mM aqueous solution of $AgNO_3$, 400 µL of a 50-mM aqueous solution of $HAuCl_4$, and 258 µL of a 100-mM solution of aqueous L-ascorbic acid are added to 40 mL of a 0.1-M aqueous solution of CTAB. After the reaction mixture turns from yellow to colorless, 48 µL of 35% HCl and 30 µL of a freshly prepared ice-cold aqueous solution of NaBH4 are added while stirring. AuNRs formed in the mixture are pelleted by centrifuging at 20,000 × g for 40 minutes at 25℃, followed by incubation at 30℃ overnight. Finally, the AuNRs are re-dispersed in about 1 mg/mL of 0.1 M CTAB.

Preparation of pm-AuNRs

pm-AuNRs were synthesized as described in our previous studies.[30,33] In brief, 1 mL of CTAB-coated AuNR (about 1 mg/mL) was centrifuged at 20,000 × g for 20 minutes at 25℃, and 900 µL of supernatants were then removed. The sample was re-dispersed with the remaining 100 µL of supernatants, diluted with 900 µL of deionized water, and then centrifuged at 20,000 × g for 20 minutes at 25℃. Subsequently, 750 µL of the supernatant was removed, and 250 µL of a 16-mg/mL sodium oleate solution was added to the samples. The mixture was heated for one hour at 50℃, and the products (oleate-coated AuNRs) were purified using a Nap5 gel column (GE Healthcare, IL, USA). Oleate-coated AuNRs were mixed with catHDL in a 1:0.4 molar ratio and heated for one hour at 50℃ in a 1.5-mL microtube. The products (pm-AuNRs) were centrifuged at 20,000 × g for 20 minutes at 25℃, and all the supernatants were carefully removed. pm-AuNRs were suspended in about I mg/mL of a 200-mM sucrose solution.

Preparation of GUVs

GUVs were prepared using the electro-formation method.[54] In a Durham tube, 40 mM of dipalmitoyl phosphatidylcholine (DPPC), DOPC, and cholesterol in chloroform were mixed with a 1-mg/mL solution of Rhodamine-PE in ethanol. A portion of the mixture (5.7 mmol of lipids)

was dropped and spread on an ITO glass (8–12 Ω/sq; Sigma-Aldrich Inc., Saint Louis, MO, USA). The ratio of DPPC to DOPC to cholesterol was 2:2:1. After heating for five minutes at 50℃, the lipid film was further spread by adding a single drop of hot chloroform, then drying in vacuo for at least two hours. The sample glass was covered with another ITO glass using a silicon sheet (about 1 mm in thickness) with a 1.5-cm square-shaped hole to create a small chamber on the lipid film. Further, 0.3×10^2 μL of a 200-mM sucrose solution was added into the chamber, and a home-made electric circuit consisting of a thin foil, the chamber, and an arbitrary function generator AFG-2005 (GW Instek, Taiwan) was made. Electric power (10 Hz, 1.4 vpp, 0.35 mV) was applied to the chamber with the arbitrary function generator at 50℃ in an ICI-1 incubator overnight. After cooling the chamber to room temperature, the dispersion of GUVs was recollected from the chamber with a disposable syringe and stored in 1.5-mL tubes at room temperature.

Observation of the phase transition process

The time-lapse observation methodology was proposed in our previous study.[30] A chamber for GUV observation was prepared by sandwiching a single silicon sheet 0.1 mm in thickness with a hole of about 6 mm between two cover glasses 0.13–0.17 mm in thickness (24 mm × 50 mm and 18 mm × 18 mm). Thereafter, 2 μL of pm-AuNRs and 2 μL of Lo/Ld GUVs were dropped in the hole, and another cover glass was gently placed on top to form a boundary between the two solutions. The area near the boundary was then observed using an LSM 800 microscope. Time-lapse imaging was performed manually to minimize photo-bleaching caused by continuous automatic imaging and to focus on the surface of floating GUVs in each image capture.

Results & Discussion

We prepared HDLs, which are composed of reconstituted Apo-AI protein and lipids, and covered the surface of the AuNR with the HDLs to form pm-AuNR as shown in Figure 1A.[34] The HDL contained POPC and DOTAP in a 7:3 molar ratio. This material shows the spontaneous Lo phase domain selective accumulation and causes Lo-to-So phase separation, as previously reported.[30]

To validate the process of phase transition, we built a small chamber with two cover glasses and a perforated silicon sheet.[30] Two dispersants of Lo/Ld GUVs and pm-AuNRs were dropped on the bottom cover glass in the perforation of the silicon sheet and were flattened with the top cover

glass to create a boundary of the two dispersants (Figure 1B). On the boundary, the pm-AuNRs were gradually dispersed into the Lo/Ld GUVs and accumulated on the Lo phase. To determine the boundary area, we searched the good GUVs to monitor the domain dynamics in high resolution. For the fluorescent observation, the Ld phase of GUVs was labeled with 1% 1,2-dioleoyl-sn-glycero-3-phosphoethanolamine-N-(lissamine rhodamine B sulfonyl) (Rho-PE), and pm-AuNRs were labeled with 6% NBD-PE. As pm-AuNRs cause cholesterol depletion, phase transition occurred on the membranes of the GUVs. Domain shape changed from circular to non-circular, which is characteristic of So/Ld GUVs (Figure 2A).

We measured the change in the domain morphology of Lo/Ld GUVs. Without pm-AuNRs, Lo/Ld GUVs had a circular domain (Figure 2B). We identified GUVs on the boundary of the two dispersants and monitored GUV domains with well-absorbed pm-AuNRs on the Lo domain. Further, we performed time-lapse imaging to minimize photo-bleaching.

At the beginning of the observation, the Lo domain had a circular phase boundary due to the line tension of the domain (Figure 2C, 0 minute). The pm-AuNRs are attached to the Lo phase region (shown in green). Some mixing of the Ld phase region labeled with Rho-DPPE (shown in brown) occurred over time as the domain boundary was destabilized. There were local ruptures on the boundary (shown in yellow), and the localized mixtures were a starting point of the mutual incursion of domains. The mixed region was torn and diffused as microdomains into the Lo phase region (Figure 2C, 2 minutes 22 seconds).

Larger morphological changes occurred in the next process. High-resolution imaging revealed the process on the boundary. After continuous penetration, the penetrated domain structure became a string and fragmented into smaller domains in the post-Lo domain region (Figure 2C). Microdomains in the late stage were larger than microdomains in the first stage. The microdomains joined and formed a new Ld phase region. The newly formed domains were not circular. Lo-to-So phase transitions were completed in this process. After nine minutes, the

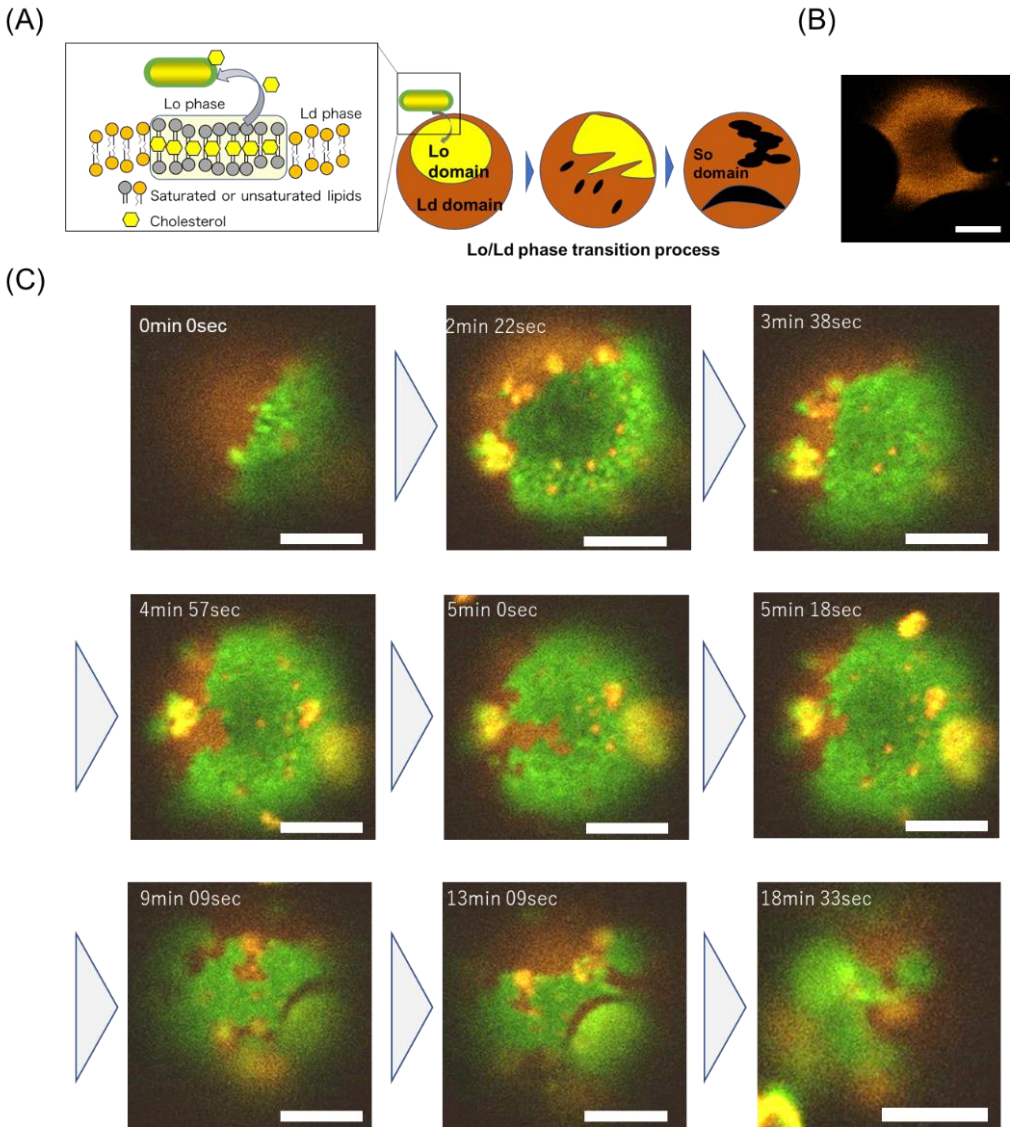

Figure 2. Analysis of Lo-to-So phase separation dynamics on GUVs caused by pm-AuNRs
(A) Schematic image of Lo/So phase transition caused by pm-AuNRs
Lo domain selective addition of pm-AuNRs induces cholesterol depletion from GUVs, resulting in So/Ld GUVs.
(B) Typical image of Lo/Ld GUVs without pm-AuNRs
Ld phase regions are stained with 0.1% Rhodamine-PE (brown). The black circle-like domains are Lo domains.
Scale bar = 5 μm
(C) Time-lapse imaging of Lo/Ld phase transition
pm-AuNRs are stained with 6% NBD-PE (green). The measurement times are shown on the upper left portion of each panel.
Scale bar = 5 μm

circular boundary collapsed, and the non-circular domain became stable. At nine minutes and nine seconds, some parts of the domain boundary showed signs of domain incursion, and a small part

of the boundaries was still ruptured. After 18 minutes, phase transition was completed, and GUVs were attached to the bottom of the cover glass, which is not an ideal condition for observation.

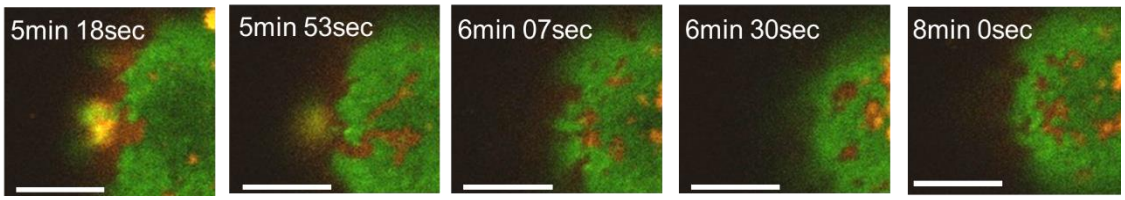

Figure 3. Analysis of Lo-to-So phase separation dynamics
The Ld domain is stained with 1% Rho-PE (brown), and pm-AuNRs are stained with 6% NBD-PE (green).
Scale bar = 2 μm

High-resolution time-lapse analysis was performed during dispersion of intruded domains (Figure 3). At 5 minutes and 18 seconds, the Lo and Ld domains intruded on each other from the region of domain rupture (shown in yellow). Regarding the Ld domain, at 5 minutes and 53 seconds, the Ld domain intruded more deeply in a stripe shape, with some parts separated from the domain. At six minutes and seven seconds, the large protruding stripe domain was completely split into small microdomains. Probably due to decrease in the line tension of the Lo/Ld domain boundary, the domains could not maintain a circular shape; but they were relatively circular due to the line tension. After two minutes, the microdomains gathered and started to form non-circular domains again. The driving force of domain re-formation was probably the decreased mobility of the green regions of GUVs caused by cholesterol depletion. The formation and deformation of domains on GUVs occurred occasionally during Lo-to-So phase transition.

To better understand the phase transition process, we tried to observe two characteristics of the process, namely domain rupture and domain incursion (Figure 4). Further, we measured the profile of fluorescent intensity. Before the start of the phase transition process, the Lo and Ld domains were separated (Figure 4A). The two domains were not mixed, even near the boundary. The Ld phase was almost only Rho-PE florescent, and the Lo phase had parts derived from pm-AuNRs that were NBD-PE fluorescent. We observed slightly high Rho-PE fluorescent intensity that was a leak of NBD-PE fluorescence in that wavelength (Figures 4B and 4C). These data were a reference for the change of domain characteristics in the steps described below.

After the start of the Lo-to-So phase transition, domain rupture and domain incursion occurred as shown in Figures 1 and 2. We evaluated the line profile of the two regions (Figure 4D). For the incursion domain, the florescent pattern was completely different in and out of the area. The intruded Ld domain showed only the Rho-PE-fluorescent region and did not show the NBD-PE-

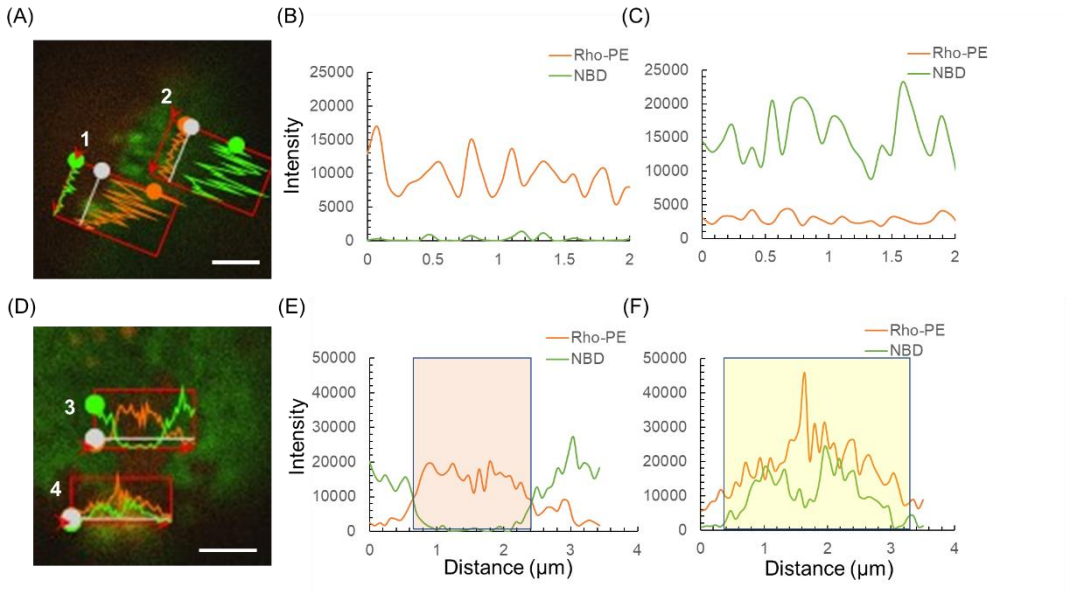

Figure 4. Typical local fluorescent intensity analysis of the boundaries of the two domains
(A) to (C): Analysis without reciprocal incursion of domains
(A) The location of florescent profiles in the Ld domain (1) and the Lo domain (2)
(B) The fluorescent profile of the Ld domain
(C) The fluorescent profile of the Lo domain
(D) to (E): Analysis with reciprocal incursion of domains
(D) The location of fluorescent proteins at incursion in the Ld domain (3) and the ruptured domains (4)
(E) The fluorescent profile of the Ld domain at the incursion region
(F) The fluorescent profile of the ruptured domains
The region of Ld incursion domain is highlighted in red.
(F) The fluorescent profile of the ruptured region
The ruptured region is highlighted in light yellow.
Scale bar = 2 μm

fluorescent region (Figure 4E). This finding indicates that domain mixture did not occur on the metamorphosed domain. In contrast, the ruptured area showed an increase in the fluorescent intensities of NBD-PE and Rho-PE. The fluorescent intensities possibly affected the rupture, resulting in phenomena such as diffraction. However, compared to other profiles, the order of intensity values was sufficient to conclude that both domains were co-localized in the ruptured area. These findings indicate that the phase transition was initiated by a mixture of the two domains in a small area and that the mixture triggered a larger domain metamorphosis via phase transition.

Finally, we observed another characteristic of phase transition, namely emitted microdomains (Figure 5A). We analyzed three other microdomains as shown in Figures 5A and 5B, and the diameter of these microdomains was around 500 nm. The size of the lipid domains was considered reasonably small, given that larger lipid rafts induced by antibody addition are of the same size.

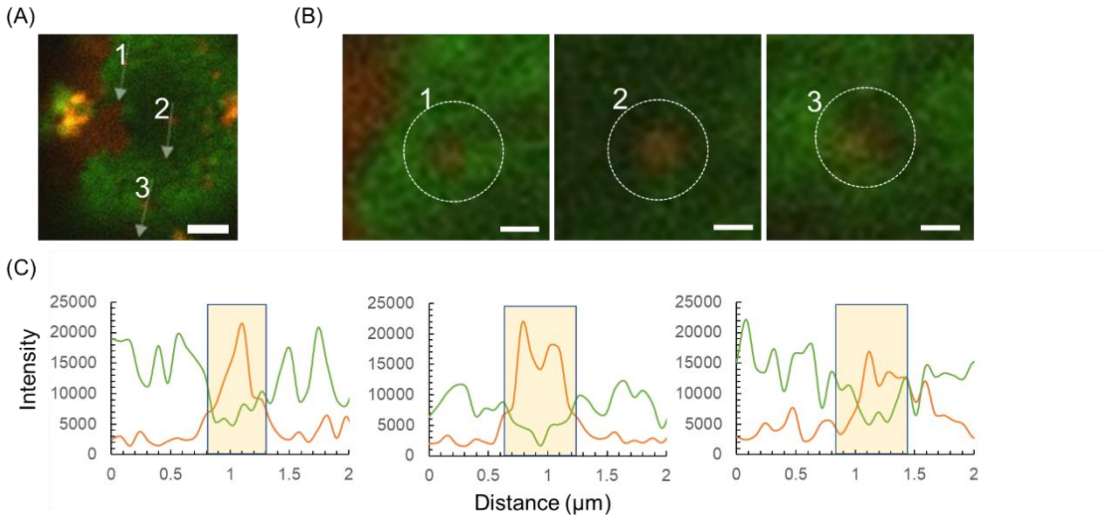

Figure 5. Fluorescent profile analysis of small microdomains from an Ld domain
(A) The location of florescent profiles at three different microdomains on a GUV (1, 2, 3)
Scale bar = 2 μm
(B) Magnified images of the microdomains
The location of each microdomain (brown) is encircled. The numbers correspond to those in (A).
Scale bar = 500 nm
(C) Fluorescent profiles of microdomains 1, 2, and 3
The microdomain regions are highlighted in light orange.

The fluorescent line profile indicated that the small microdomains have liquid order but include a small amount of pm-AuNRs. The main fluorescent intensities were those of Rho-PE, and the peak width of the Rho-PE profiles was reasonable judging from the domain size, but the domain NBD-PE fluorescent decrease was not strong compared to the profiles of the Ld phase before phase transition shown in Figure 4B.

We measured the ratio of fluorescent intensity of all the microdomains each time (Figure 6). There was variation in the ratio, but in general, the variation was between 0.5 and 1.5. This finding corresponds with the line profile shown in Figure 5 and suggests the co-existence of a part of the pm-AuNRs. The incursion domains show over 1000 values for relative ratio. The microdomain boundary may not be solid as the microdomains include some parts of Lo/So domains.

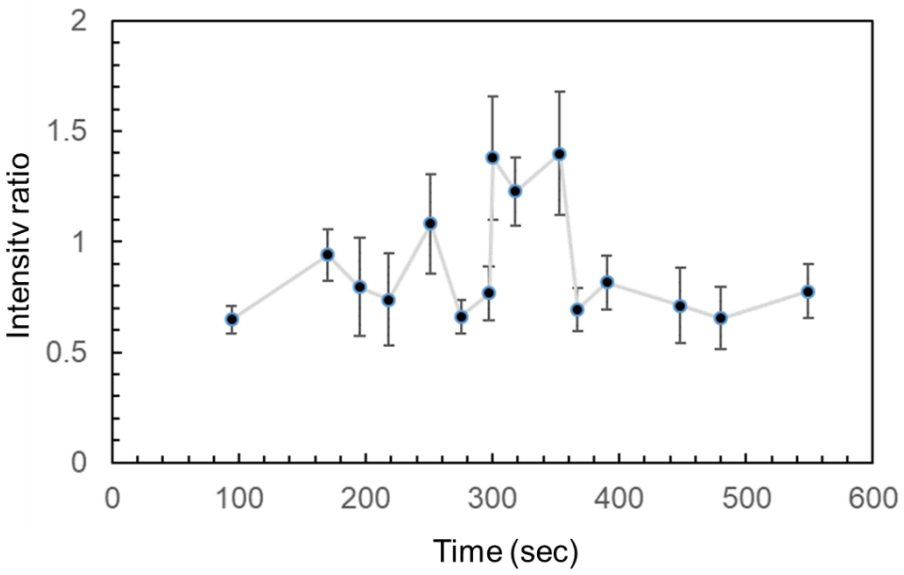

Figure 6. The florescent intensity ratio of Rho-PE to NBD-PE on microdomains in the time-course. Error bar is mean S.D.

We investigated the phase transition process of a model lipid raft caused by pm-AuNRs, which are model lipid raft manipulators. We performed time-lapse measurement and analysis of the Lo-to-So phase transition process.

Our results suggest that membrane rupture was the first process to occur following decrease of line tension due to cholesterol depletion. Destabilization of domain boundary due to lack of line tension strength was observed in giant plasma membrane vesicles.[37] In previous studies, fluctuations were monitored using increase in temperature. Our experiment was performed at room temperature, and the reason for phase transition was different, but the domain metamorphoses had common characteristics.

Cholesterol depletion also occurred by small host molecules such as methyl-beta-cyclodextrin (mBCD).[38] Previous studies have reported phase transition of mBCD and human HDL.[39,40] However, phase transition in previous studies varied in a few ways from that observed in our study. First, in our previous study, we reported that phase transition of mBCD and HDL occurred at a speed lower than that of phase transition driven by pm-AuNRs. The pm-AuNRs attached immediately to the Lo domain, and it was difficult to detect phase transition without careful observation of the boundaries of the two dispersants, but with mBCD and HDL, several minutes or hours are required before phase transition is observed. Second, in this study, domain incursion

and microdomain emission were not observed (Figure 2). In our previous study, we found that mBCD and HDL did not show domain incursion for the same GUVs as pm-AuNRs. This disparity may be explained by material adhesion. Further, it was reported that charged nanomaterials caused re-orientation of the lipid head group.[41] The above findings have not been observed in large lipid membranes, but they are plausible hypotheses.

The protruded Ld phase domain has only Ld phase characteristics (Figure 4), but the emitted microdomain appears to have a mixture of Ld and Lo phase characteristics even though the Rho-PE fluorescence was stronger than the NBD-PE fluorescence of pm-AuNRs (Figures 5 and 6). We could not determine whether phospholipids or cholesterols were mixed well or separated in smaller clusters, but we observed that they were not isolated completely as in larger domains on GUVs. This non-solidified characteristic may be important for phase transition.

Generally, on the domain boundary, line tension was maintained due to the difference in the thickness of the lipid bilayers.[42] The reduced energy caused by line tension tends to increase the domain size and reduce total boundary length and electrostatic repulsion, which tends to decrease the domain size.[43] The collapse of the domain boundary indicates that a reverse phenomenon occurred. Thus, cholesterol depletion from the Lo domain caused by pm-AuNRs reduced the line tension, and due to lack of cholesterol, the small microdomains did not maintain sufficient line tension, so they fused with each other, causing the domain to metamorphosize.

Previous studies investigated the interference of lipid rafts by adhesive polymers or bio-macromolecules, including synthesized macromolecules,[44] lactoferrin,[45] and amyloid proteins.[46,47] Our findings regarding the non-equilibrium process can inform a more suitable strategy for the use of lipid raft manipulators in cell engineering.

The non-equilibrium process described in this study can occur on the lipid bilayer membranes of living cells. The regulation of lipid rafts on living cells remains a controversial topic,[48] but cholesterol depletion or supplementation constantly occurs as HDL is essential for the functions of T cells, B cells, and macrophages.[35,49] Recent studies have reported that the formation of cholesterol-rich areas may lead to protein and ganglioside clustering to form real lipid rafts in cells;[50,51] thus, the formation/deformation of cholesterol-rich areas on plasma membranes is an important process. Membrane–material interfaces have been reported to play a significant role in lipid raft formation. Some previous studies focused on actin filaments as lipid raft regulators to analyze raft–material interaction.[52] The results of our study provide deeper insight into the process of lipid raft formation/deformation through interaction with external materials.

Conclusions

In summary, we observed and analyzed Lo-to-So phase transition in the model lipid raft domain of GUVs induced by pm-AuNRs. The domain boundary was fragile, and domains were mixed at some points on the boundary. Domain protrusion and tearing resulted in some microdomains that grouped together. The microdomains tended to be mixtures of Lo phase and Ld phase lipids. Our study findings indicate that cholesterol depletion resulted in decrease of the line tension of the Lo domain, which maintained the Lo domain shape. These findings can be useful for the design of a new model lipid raft manipulator. They can also provide a clearer understanding of the regulation of lipid rafts in living cells, which may include cholesterol depletion and interaction with external materials.

Author Contributions

T.M brought the idea of this research, conducted all experiments and analysis and wrote the first draft of the research. T.M and M.T. had discussed the results and polished the draft to submit. A part of this research is included in the Ph.D thesis of T.M.

Conflicts of interest

The authors declare no conflicts of interest.

Acknowledgments

This work was supported by JSPS KAKENHI Grant Numbers JP19J14903 and 21J00852. We wish to appreciate Toyama Prefectural University and Tsukuba University for their kind support of the research. We are grateful for the academic and supportive atmosphere of Kumano Dormitory Community at Kyoto University. We thank to Koji Takata for transition electron microscopy observation for AuNRs and Kentaro Shiraki for some advice.

References

1. G. V. van Meer, D. R. Voelker and G. W. Feigenson, *Nat. Rev. Mol. Cell Biol.*, 2008, **9**, 112–124.
2. F. A. Heberle and G. W. Feigenson, *Cold Spring Harb. Perspect. Biol.*, 2011, **3**.

3. J. M. Steim, M. E. Tourtellotte, J. C. Reinert, R. N. McElhaney and R. L. Rader, *Proc. Natl. Acad. Sci. U. S. A.*, 1969, **63**, 104–109.

4. D. Chapman and J.Urbina, *J. Biol. Chem.*, 1974, **249**, 2512–2521.

5. R. D.Klausner, A. M.Kleinfeld, R. L.Hoover and M. J.Karnovsky, *J. Biol. Chem.*, 1979, **255**, 1286-1295.

6. M. J.Karnovsky, A. M.Kleinfeld, R. L.Hoover and R. D.Klausner, *J. Cell Biol.*, 1982, **94**, 1–6.

7. K. Simons and E. Ikonen, *Nature*, 1997, **387**, 569–572.

8. O. Wesołowska, K. Michalak, J. Maniewska and A. B. Hendrich, *Acta Biochim. Pol.*, 2009, **56**, 33–39.

9. H. A. Anderson, P. A. Roche and MHC, *Biochim. Biophys. Acta*, 2015, **1853**, 775–780.

10. S. Mahammad, J. Dinic, J. Adler and I. Parmryd, *Biochim. Biophys. Acta*, 2010, **1801**, 625–634.

11. P. Varshney, V. Yadav and N. Saini, 2016, **1**, 13-24.

12. R. Dirkx, Jr and M. Solimena, *J. Diabetes Investig.*, 2012, **3**, 339–346.

13. J. Colin, L. Gregory-Pauron, M. C. Lanhers, T. Claudepierre, C. Corbier, F. T. Yen, C. Malaplate-Armand and T. Oster, *Biochimie,* 2016, **130**, 178-187.

14. T. Murai, *Int. J. Cell Biol.*, 2012, **2012**, 763283.

15. É. Sághy, É. Szőke, M. Payrits, Z. Helyes, R. Börzsei, J. Erostyák, T. Z. Jánosi, G. Sétáló Jr and J. Szolcsányi, *Pharmacol. Res.*, 2015, **100**, 101–116.

16. **C.** Morenilla-Palao, **M.** Pertusa, **V.** Meseguer, **H.** Cabedo and **F.** Viana, *J. Biol. Chem.*, 2009, **284**, 9215–9224.

17. M. Sorice, R. Misasi, G. Riitano, V. Manganelli, S. Martellucci, A. Longo, T. Garofalo and V. Mattei, *Front. Cell Dev. Biol.*, 2020, **8**, 618296.

18. S. T. Yang, V. Kiessling, J. A. Simmons, J. M. White and L. K. Tamm, *Nat. Chem. Biol.*, 2015, **11**, 424–431.

19. A. Mamode Cassim, P. Gouguet, J. Gronnier, N. Laurent, V. Germain, M. Grison, Y. Boutté, P. Gerbeau-Pissot, F. Simon-Plas and S. Mongrand, *Prog. Lipid Res.*, 2019, **73**, 1–27.

20. M. Sorice, V. Mattei, P. Matarrese, T. Garofalo, A. Tinari, L. Gambardella, L. Ciarlo, V. Manganelli, V. Tasciotti, R. Misasi and W. Malorni, *Commun. Integr. Biol.*, 2012, **5**, 217–219.

21. M. A. Surma, C. Klose and K. Simons, *Biochim. Biophys. Acta*, 2012, **1821**, 1059–1067.

22. V. N. Nesterov, I. S. Nesterkina, O. A. Rozentsvet, N. V. Ozolina and R. K. Salyaev, *Dokl. Biochem. Biophys.*, 2017, **476**, 303–305.

23. G. Staneva, N. Puff, M. Seigneuret, H. Conjeaud and M. I. Angelova, *Langmuir*, 2012, **28**, 16327–16337.

24. J. D. Nickels, X. Cheng, B. Mostofian, C. Stanley, B. Lindner, F. A. Heberle, S. Perticaroli, M. Feygenson, T. Egami, R. F. Standaert, J. C. Smith, D. A. Myles, M. Ohl and J. Katsaras, *J. Am. Chem. Soc.*, 2015, **137**, 15772–15780.

25. C. C. Vequi-Suplicy, K. A. Riske, R. L. Knorr and R. Dimova, *Biochim. Biophys. Acta*, 2010, **1798**, 1338–1347.

26. E. S. Wu, K. Jacobson and D. Papahadjopoulos, *Biochemistry*, 1977, **16**, 3936–3941.

27. M. Ma and D. Bong, *Acc. Chem. Res.*, 2013, **46**, 2988–2997.

28. C. M. Rosetti, A. Mangiarotti and N. Wilke, *Biochim. Biophys. Acta Rev. Biomembr.*, 2017, **1859**, 789–802.

29. W. F. Bennett and D. P. Tieleman, *Biochim. Biophys. Acta*, 2013, **1828**, 1765–1776.

30. T. Nobeyama, K. Shigyou, H. Nakatsuji, H. Sugiyama, N. Komura, H. Ando, T. Hamada and T. Murakami, 2020, **26**, 7741-7746.

31. J. K. Sheavly, J. A. Pedersen and R. C. Van Lehn, *Nanoscale*, 2019, **11**, 2767–2778.

32. A. Ridolfi, L. Caselli, C. Montis, G. Mangiapia, D. Berti, M. Brucale and F. Valle, *J. Microsc.*, 2020, **280**, 194–203.

33. T. Nobeyama, M. Mori, K. Shigyou, K. Takata, G. N. Pandian, H. Sugiyama and T. Murakami, *ChemistrySelect*, 2018, **3**, 8325-8331.

34. H. Nakatsuji, T. Numata, N. Morone, S. Kaneko, Y. Mori, H. Imahori and T. Murakami, *Angew. Chem. Int. Ed. Engl.*, 2015, **54**, 11725–11729.

35. E. Grao-Cruces, S. Lopez-Enriquez, M. E. Martin and S. Montserrat-de la Paz, *Int. J. Biol. Macromol.*, 2022, **195**, 117–123.

36. E. C. Dreaden, A. M. Alkilany, X. Huang, C. J. Murphy and M. A. El-Sayed, *Chem. Soc. Rev.*, 2012, **41**, 2740–2779.

37. P. C. Sarah, L. Veatch, P. Sengupta, A. Honerkamp-Smith, D. Holowka and B. Baird, *ACS Chem. Biol.*, 2008, **3**, 287–293-293.

38. R. Zidovetzki and I. Levitan, *Biochim. Biophys. Acta*, 2007, **1768**, 1311–1324.

39. S. A. Sanchez, G. Gunther, M. A. Tricerri and E. Gratton, *J. Membr. Biol.*, 2011, **241**, 1–10.

40. N. Puff, A. Lamazière, M. Seigneuret, G. Trugnan and M. I. Angelova, *Chem. Phys. Lipids*, 2005, **133**, 195–202.

41. B. Wang, L. Zhang, S. C. Bae and S. Granick, *Proc. Natl. Acad. Sci. U. S. A.*, 2008, **105**, 18171–18175.

42. P. I. Kuzmin, S. A. Akimov, Y. A. Chizmadzhev, J. Zimmerberg and F. S. Cohen, *Biophys. J.*, 2005, **88**, 1120–1133.

43. A. J. García-Sáez, S. Chiantia and P. Schwille, *J. Biol. Chem.*, 2007, **282**, 33537–33544.

44. G. Li, T. Sasaki, S. Asahina, M. C. Roy, T. Mochizuki, K. Koizumi and Y. Zhang, *Chem.*, 2017, **2**, 283-298.

45. C. Santos-Pereira, M. T. Andrés, S. R. Chaves, J. F. Fierro, H. Gerós, S. Manon, L. R. Rodrigues and M. Côrte-Real, *Int. J. Biol. Macromol.*, 2021, **171**, 343–357.

46. F. Malchiodi-Albedi, V. Contrusciere, C. Raggi, K. Fecchi, G. Rainaldi, S. Paradisi, A. Matteucci,

M. T. Santini, M. Sargiacomo, C. Frank, M. C. Gaudiano and M. Diociaiuti, *Biochim. Biophys. Acta*, 2010, **1802**, 406–415.

47. D. R. Taylor and N. M. Hooper, *Mol. Membr. Biol.*, 2006, **23**, 89–99.

48. E. Sezgin, I. Levental, S. Mayor and C. Eggeling, *Nat. Rev. Mol. Cell Biol.*, 2017, **18**, 361–374.

49. D. J. Rader, *J. Clin. Invest.*, 2006, **116**, 3090–3100.

50. N. Komura, K. G. Suzuki, H. Ando, M. Konishi, M. Koikeda, A. Imamura, R. Chadda, T. K. Fujiwara, H. Tsuboi, R. Sheng, W. Cho, K. Furukawa, K. Furukawa, Y. Yamauchi, H. Ishida, A. Kusumi and M. Kiso, *Nat. Chem. Biol.*, 2016, **12**, 402–410.

51. K. G. Suzuki, R. S. Kasai, K. M. Hirosawa, Y. L. Nemoto, M. Ishibashi, Y. Miwa, T. K. Fujiwara and A. Kusumi, *Nat. Chem. Biol.*, 2012, **8**, 774–783.

52. S. Bodin, C. Soulet, H. Tronchère, P. Sié, C. Gachet, M. Plantavid and B. Payrastre, *J. Cell Sci.*, 2005, **118**, 759–769.

53. N. R. Jana, *Small*, 2005, **1**, 875–882.

54. T. Hamada and K. Yoshikawa, *Cells, Mater.*, 2012, **5**, 2292-2305.